Journal of Materials Chemistry B

Accepted Manuscript

ROYAL SOCIETY OF CHEMISTRY

www.rsc.org/materialsB

Journal of Materials Chemistry B

Cite this: DOI: 10.1039/c0xx00000x

www.rsc.org/xxxxxx

Paper

Peptide Amphiphiles with Multifunctional Fragments Promoting Cellular Uptake and Endosomal Escape as Efficient Gene Vectors

Liang Luan[a], Qingbin Meng[a], Liang Xu[a], Zhao Meng[a], Husheng Yan*[b] and Keliang Liu*[a]

Received (in XXX, XXX) Xth XXXXXXXXX 20XX, Accepted Xth XXXXXXXXX 20XX

DOI: 10.1039/b000000x

To overcome barriers associated with gene delivery, a series of peptides consisting of multifunctional fragments, including a cationic amphiphilic α-helical antimicrobial peptide (AMP), the cell penetrating peptide (CPP), TAT, a stearyl moiety, and cysteine residues, were designed and synthesized for evaluation as non-viral gene vectors. TAT and AMP segments were utilized to mediate cellular uptake and endosomal escape, respectively. Stearyl moieties provide an intramolecular hydrophobic environment to promote AMPs to form an α-helical conformation in PBS, and this is beneficial for DNA binding, cellular uptake, and endosomal escape. The α-helical content of the peptides, as well as the particle size, zeta potential, and morphology of the peptide/DNA complexes, were characterized. Fluorescence activated cell sorting (FACS) and confocal microscopy data showed that the peptides were able to efficiently translocate a pGL3 control plasmid across the plasma membrane via endocytosis, and then they successfully evaded endosomal entrapment and possible metabolic degradation. Moreover, one of the peptide vectors exhibited a high transfection efficiency similar to that of Lipofectamine 2000, concomitant with lower cytotoxicity. Overall, a combination of the four functional segments tested was used to generate a non-viral gene vector that synergistically promoted cellular uptake, endosomal escape, and gene expression.

Introduction

Gene therapy has gained significant attention over the past two decades as a method for treating genetic disorders such as cancer, monogenetic diseases, cardiovascular diseases, and other conditions.[1,2] Unfortunately, the cellular uptake of free oligonucleotides and plasmid DNA is hindered by the large size and negative charge of these complexes. Moreover, these complexes are rapidly degraded by ribozymes in an acidic environment.[3,4] Thus, a safe and effective gene delivery system has remained a barrier to effective gene therapy for many years. Viral vectors can be used as gene delivery systems due to their high transfection efficiency.[5] However, their disadvantages include toxicity, immunogenicity, and limitations with respect to scale-up.[6] Therefore, non-viral vectors, including cationic lipids, polymers, and peptides, have been designed and engineered to overcome the limitations associated with viral vectors. However, *in vitro* and *in vivo* barriers such as DNA complexation, cellular uptake, endosomal escape, cytoplasmic mobility, and nuclear entry remain to be addressed.[6,7]

In recent years, peptides have been developed as an alternative to non-viral vectors due to their ability to mediate various biological functions, including cell penetration,[8] targeting,[9] and endosomal escape.[10,11] In particular, cell penetrating peptides (CPPs) are short peptides (< 30 amino acids) that mostly contain arginine and/or lysine residues, and have been shown to provide efficient cell penetration and intracellular accumulation. The CPP HIV-TAT is derived from the HIV Tat protein and has the sequence, *GRKKRRQRRR* (aa 48-57). This TAT peptide can bind and condense DNA using electrostatic interactions and can translocate exogenous DNA across plasma membranes via endocytosis.[8,12] However, TAT peptide-mediated endocytosis generally results in the localization of peptide/DNA complexes to endosomes, and their eventual degradation in lysosomes.[8,11-13] Therefore, the efficient delivery of exogenous DNA into the cytosol requires peptides that are capable of endosomal entry and escape. Cationic amphiphilic α-helical antimicrobial peptides (AMPs) are one type of peptides that exhibit membrane-disrupting properties.[10,14,15] AMPs are usually disordered in aqueous solution, yet assume an α-helical secondary structure in a hydrophobic environment. In particular, at low peptide/lipid ratios, peptides preferentially align perpendicularly to the cell membrane and then eventually insert into the bilayer. This causes a thinning of the chain region, increased internal membrane tension, and an increase in the peptide/lipid ratio. The peptides then preferentially bind to the edges of pores in the membrane, thereby loosening the tension in the internal membrane.[15,16] Hydrophobic modifications of peptides have also been shown to enhance the cellular uptake and endosomal escape of peptide/DNA complexes by facilitating the absorption of complexes by membranes via their hydrophobic moieties.[17,18] In particular, stearylation can provide a hydrophobic environment intramolecularly. For example, a stearyl moiety at the N-terminus of an AMP was found to increase the α-helical content of the

peptide in aqueous solution.[19,20] Stearylated AMPs adopt a secondary amphiphilic α-helical structure that the non-polar face of the AMPs self-assemble inside while the cationic amino acids extend into the aqueous environment. As a result, plasmid DNA binding ability and cellular uptake efficiency are enhanced.[21] The incorporation of cysteine residues into peptides can also increase α-helical content, possibly due to the increased size of the peptide molecule and cysteine not belonging to the helical breaker amino acids. This increase in size can serve to enhance hydrogen bonding interactions between the carbonyl O atom of an amino acid position (*i*) and a subsequent amide proton of the (i + 4) amino acid position in the peptide backbone.[22] Similarly, an increased number of repeat units (n) also increases the a-helical folding by the same virtue, which is characterized by the extent of the negative values of the molecular elipticity at the minima points. The presence of cysteine residues also increases the potential for crosslinking to occur via disulfide bonds in acidic endosomes or lysosomes, and improves the stability of peptide/DNA complexes in the extracellular environment. For example, when cysteine residues were added to link low molecular weight (LMW) peptides via reducible disulfide bonds, cellular uptake and gene transfection efficiency of these peptides was enhanced.[23,24]

In the present study, a series of peptides containing different functional segments were designed and synthesized to enhance gene delivery (Fig. 1A and B). The peptides included a DNA binding segment (containing positively charged amino acids such as lysine and arginine), a cell penetrating segment (e.g., the TAT sequence), and an endo-lysosomal membrane disrupting segment (e.g., $(LLKK)_3$ which provides anamphiphilic α-helical conformation that disrupts membranes).[25] To promote associations with the hydrophobic cellular membrane and to increase cationic charge density, a stearyl group was conjugated to the N-terminus of the peptides, which was previously shown to increase the α-helical content of peptides in aqueous solution.[26] Two cysteine residues were also incorporated at the terminus of each $(LLKK)_3$ segment to increase α-helical content and the cysteine residues coupled to N- terminus provide thiol groups for crosslinking.[22] In addition, non-polar hydrophobic leucine residues that are present would be predicted to associate with the inside of the multi-helix conformation, while cationic hydrophilic lysine residues would extend into the aqueous solution to increase cationic charge density. It is hypothesized that the peptide that incorporates all of the above features will provide effective condensation of DNA into a complex, and this will markedly improve cellular uptake and endosomal escape to improve gene expression efficiency. Fig. 1C provides an overview of the four peptide/DNA complexes that were evaluated for cellular uptake and endosomal escape via endocytosis. Lipofectamine™ 2000 (Lip2000) was used as a positive control and lysosomotropic agents, such as chloroquine (CQ), were not needed. It is anticipated that the structural and multifunctional features evaluated in the present study will provide a promising gene delivery system for further investigation.

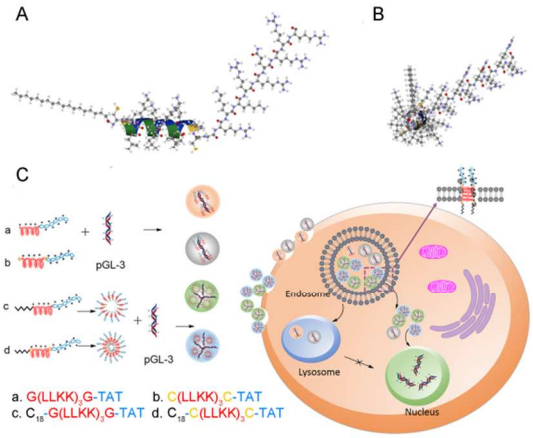

Fig.1 An overview of the peptide-based gene delivery systems evaluated in this study. (A) A structural representation of C_{18}-C$(LLKK)_3$C-TAT shows the α-helical backbone of $(LLKK)_3$ and the distribution of TAT and cysteine residues. (B) A representation of the side chain orientations for the main helical backbone. (C) A schematic illustration of the plasmid DNA condensation and gene delivery mediated by each of the TAT peptide-based gene vectors.

Experimental

Materials

N-fluorenyl-9-methoxycarbonyl (Fmoc)-protected L-amino acids were purchased from GL Biochem Ltd. (Shanghai, China). Rink amide resin (0.44 mmol/g) was purchased from Nankai Hecheng (Tianjin, China). 2-(1H-benzotriazole-1-yl)-1,1,3, 3-tetramethyluronium hexafluorophosphate (HBTU), hydroxybenzotriazole (HOBT), diisopropyylethylamine (DIEA), trifluoroacetic acid (TFA), thioanisole, ethandithiol, and anisole were purchased from Sigma-Aldrich (Shanghai, China) and were used without further purification. All other solvents were redistilled from drying reagents.

Dulbecco's Modified Eagle Medium (DMEM) was purchased from HyClone (Beijing, China). Fetal bovine serum (FBS), penicillin-streptomycin, and phosphate buffered saline (PBS) were purchased from Invitrogen (CA, USA).The pGL3 control vector, the Dual-Glo® Luciferase Assay System, and the CellTiter 96®AQ_{ueous}One Solution Cell Proliferation Assay were purchased from Promega (WI, USA). The QIAfilter plasmid purification Giga Kit was purchased from Qiagen (Hilden, Germany). The intercalating dye, YOYO®-1 Iodide (491/501), was purchased from Invitrogen. A Bradford protein assay kit was purchased from Beijing Solarbio Science &Technology Co., Ltd. (Beijing, China).

Peptide synthesis and purification

All peptides were prepared by solid-phase synthesis using Fmoc chemistry on an automatic Liberty-12-Channel Automated Peptide Synthesizer with an integrated microwave system (CEM, USA). In the presence of DIEA/HBTU/HOBT, amino acids were coupled to the Rink amide resin (0.44 mmol/g). To remove the Fmoc protected groups, 20% piperidine/DMF (v/v) solution was introduced to the resin. Cleavage of targeted peptides and deprotection of side chain protected residues were performed with 10 mL TFA/thioanisole/ethandithiol/anisole (90/5/3/2) for 0.5 h at 0 °C, followed by an incubation for 2.5 h at room

temperature (RT).

Crude peptides were purified using Reverse-Phase High Performance Liquid Chromatography (RP-HPLC) with an XBridge™ preparative C8 column (Waters, USA) and a linear gradient of acetonitrile and deionized (DI) water containing 0.1% (v/v) TFA. The molecular weights of the peptides were measured using Matrix-Assisted Laser Desorption/Ionization Time of Flight Mass Spectrometry (MALDI-TOF-MS) with a Bruker Reflex mass spectrometer (Bruker Daltonics, Inc., CA, USA).

Circular dichroism (CD) measurements

CD spectra (190–260nm) were recorded with a Biologic MOS-450 (Claix, France) using the following conditions: speed: 50nm/min, time response: 2 s, resolution: 0.5 nm, bandwidth: 4.0 nm, and a 1-mm path cell. Peptides at a concentration of 50nM were in PBS buffer (pH 7.4) or 50% TFE in PBS. Spectra were baseline-corrected by subtracting the blank spectrum obtained for a sample containing all components except the peptide.

Preparation of vector/DNA complexes

Peptide/DNA binary complexes at various charge ratios (N/P) ranging from 2 to 8 were prepared by adding 1.0 μg pGL3 control DNA (in 25 μL PBS) into the corresponding amount of peptide solution (in 25 μL PBS). After vortexing the mixtures for 5 s, these mixtures were incubated at 37 °C for 30 min to allow the complexes to form, and then they were diluted to a total volume of 500 μL in DMEM without serum. DNA complexes were prepared in parallel with Lip2000 according to the manufacturer's instructions (Invitrogen). A DNA solution (1.0 μg) was also diluted in DMEM without serum medium (100 μL) as a control. The amount of Lip2000 to produce the required weight ratio was diluted in DMEM without serum medium, and then it was added to the DNA solution, mixed gently, and incubated at RT for 30 min.

Agarose gel electrophoresis assay

Peptide/DNA complexes at a N/P ranging from 0 to 3 were prepared as described above with the dropwise addition of 0.1 μg pGL3 DNA into the peptide solutions. The complexes were then diluted to a constant volume of 10 μL and were loaded onto a 1% (w/v) agarose gel in tris-acetate-ethylenediaminetetraacetic acid (TAE) buffer. After undergoing electrophoresis at 100 V for 60 min, the gels were stained with ethidium bromide (EtBr, 1.0 μg/mL) for 15 min. DNA was visualized under an ultraviolet lamp using a ChampGel 6000 system (Beijing Sage Creation Science and Technology Co., Ltd., Beijing, China).

Particle size and zeta potential measurements

Particle size and zeta potential were measured using dynamic light scattering (DLS) (Zetasizer Nano ZS90, Malvern, UK) with a fixed scattering angle of 90º at 25ºC. Peptide/DNA binary complexes were prepared at N/P ratios ranging from 2 to 8 by adding 2.0 μg pGL3 to an appropriate volume of peptide solution. The prepared complexes were incubated at 37 °C for 30 min, then were diluted to a 1.0 mL volume with PBS or purified water for particle size measurements and zeta potential measurements, respectively.

Transmission electron microscopy (TEM)

The morphologies of the peptide/DNA complexes at N/P ratios 4 were observed by TEM (Hitachi H-7650 microscope, Tokyo, Japan). The complexes were prepared by adding 1.0 μg pGL3 solution to each peptide solution as appropriate. The complexes were then diluted to a constant volume of 500 μL with deionized (DI) water. After an incubation at 37 °C for 30 min, the peptide/DNA complex solutions were dropped onto a copper mesh and dried under a light before being examined.

Cell culture and cytotoxicity assays

293T cells and NIH-3T3 cells were cultured in DMEM supplemented with 10% FBS and 1% penicillin-streptomycin (10 000 U/mL) in a humidified atmosphere of 5% CO_2 at 37°C.

Cytotoxicity of the peptides and peptide/DNA complexes were evaluated in 293T cells and NIH-3T3 cells by Owen's reagent (MTS) assay. Briefly, both cell types were seeded in 96-well plates (1×10^4cells/well) with 100μL DMEM supplemented with 10% FBS. After 24h, each set of cells was treated with the appropriate concentration of peptide or peptide/DNA complex in 100 μL medium without serum. After 4 h, the cells received fresh medium and were incubated for another 20 h. The medium was then removed, the cells were washed twice with PBS, and 20 μL CellTiter 96®AQ_{ueous}One Solution reagent plus 80 μL PBS was added to each well. After 1 h at 37 °C, absorbance values for each well were measured at 490 nm using a SpectraMax® M5 (Molecular Devices, WI, USA). Cells containing PBS alone were used as a negative control. Cell viability data were obtained by calculating the ratio of viable cells in the treated cultures to untreated control cells. This experiment was repeated five times for each peptide concentration.

Calcein release assays

Liposome leakage assay

Liposomes were prepared using a repeated freeze-thaw method following extrusion.[27] Briefly, 10 mg POPC and 1.9 mg cholesterol in 1 mL chloroform was placed in a 50 mL glass bottle and was reduced to a thin film in a rotary evaporator under vacuum. Each lipid was hydrated in 1.0 mL of a solution containing 60 mM calcein, 200 mM NaCl, and 20 mM HEPES. After seven freeze-thaw cycles, the liposomes were extruded through a 200 nm polycarbonate membrane under high pressure (Avanti, AL, USA) at RT. Free calcein was removed by gel exclusion chromatography using a Sephadex G-50 column (J&K Scientific Ltd., Shanghai, China). The concentration of each phospholipid preparation was determined using a Stewart assay.[28] Briefly, 10 μL of 0.1 nmol peptides or peptide/DNA (N/P =4) complexes were added into 96-well optical plates (Thermo, NY, USA) containing 180 μL 200 mM NaCl/citrate buffer (PH 5) and 10 μL calcein liposomes (0.5 mg/mL). After 30 min at RT, calcein release was measured based on fluorescence emissions detected at 515 nm (excitation 490 nm) using a SpectraMax® M5 (Molecular Devices). As a positive control, 100% calcein leakage (I_∞) was achieved following treatment with 0.1% Triton X-100, while untreated calcein liposomes in citrate buffer were used as a negative control (I_0). Initial calcein fluorescence (I_t) was subtracted from the total fluorescence mediated by each peptide or peptide/DNA complex and then the data were plotted as a percentage of total fluorescence of 100% calcein leakage to the untreated liposomes (R_t): $R_t = 100 \times (I_t - I_0) / (I_\infty - I_0)$.

Calcein release assay in cells[29]

Briefly, 293T cells and NIH-3T3 cells were seeded in 15 mm glass bottom culture dishes (NEST, Shanghai, China) (3×10^4 cells/mL) containing glass cover slips After 24 h, the medium was replaced with 1ml DMEM containing 0.2 mg/ml calcein (TCI, Tokyo, Japan) with or without peptides. After 30 min, the medium was removed and the cells were washed twice with PBS. Using a 60× oil immersion lens of an inverted microscope (PerkinElmer UltraView Vox, PerkinElmer, UK) equipped with cover slip chambers at 37°C in a humidified atmosphere of 5% CO_2, spinning disk confocal microscopy was performed using a 488 nm laser excitation.

***In vitro* transfection**

The transfection efficiency of each peptide/DNA complex was evaluated in 293T cells and NIH-3T3 cells. Briefly, cells were seeded in 24-well plates (5×10^4 cells/well) in 500μL DMEM containing 10% FBS at 37 °C in 5% CO_2 atmosphere overnight to reach 80% confluence. The peptide/DNA complexes were prepared at various N/P ratios as mentioned above, and were diluted to 500 μL in serum-free DMEM. The cells were then cultured with complexes in serum-free DMEM. After 4 h, the medium was replaced with 1.0 mL fresh DMEM containing 10% FBS and the cells were cultured for an additional 44 h. Lip2000 was used as a positive control according to the manufacturer's instructions.

For the luciferase assays, the culture medium was discarded, cells were washed with PBS, and cell culture lysis reagent (100 μL, Promega) was added to each well. After 15 min at RT, luciferase activity was measured using a luciferase assay kit (Promega) and was normalized to the total protein content of each cell lysate as determined by a Bradford protein assay. Relative light units (RLUs) were measured using a SpectraMax® M5 (Molecular Devices) with a 500 ms read time.

For the CQ experiments, transfections were performed as described above, except that cells were pre-incubated with 100 μmol CQ (TCI, Tokyo, Japan) for 15 min at 37 °C before the peptide/DNA complexes were added, and it was also added during each transfection.

For the experiments involving endocytosis inhibitors, cells were pre-treated with the inhibitors as appropriate: chloropromazine hydrochloride (CPZ, 10 μg/ml), amiloride (50□M), or methyl-beta-cyclodextrin (MβCD, 5 mM). After 30 min, transfections were performed as described above.

Fluorescence-activated cell sorter (FACS) analysis

NIH-3T3 cells were seeded in 12-well plates (8×10^4 cells/well) 24 h before transfection. The pGL3 control plasmid (1 μg) was labeled with 2.5 μL YOYO-1 (10 μM) at 37 °C for 30 min before peptide was added. Peptide/DNA complexes were then prepared at various N/P ratios as mentioned above, and then were added into each well. After 4 h, the medium was removed, the cells were washed three times with PBS containing 2 mg/ml heparin sodium, the cells were treated with 0.02% (w/v) EDTA and 0.25% (w/v) trypsin solutions for 1 min, and then were harvested in 200 μL ice-cold PBS. Fluorescence analysis was performed immediately afterwards and a minimum of 15,000 events/sample were analyzed using a FACS (Becton Dickinson, NJ, USA) (Ex 488 nm, Em 530 nm).

To study the mechanism(s) responsible for the cellular uptake of peptide/DNA complexes, NIH-3T3 cells were pre-treated with an endocytosis-specific inhibitor [CPZ (10 μg/ml), amiloride (50 μM), or (MβCD, 5 mM)] for 30 min. The cells were then incubated with YOYO-1-labeled peptide/DNA complexes at a N/P ratio of 4. After 4 h, the cells were washed with PBS containing 2 mg/ml heparin sodium three times, they were treated with 0.02% (w/v) EDTA and 0.25% (w/v) trypsin solutions for 1 min, and then were harvested in 200 μl PBS and analyzed as described above.

Confocal microscopy

Both 293T cells and NIH-3T3 cells were seeded in 15 mm glass bottom culture dishes (NEST) containing glass cover slips (3×10^4 cells/mL). After 24 h, the complexes were prepared as described in **FACS analysis** section. The complexes were supplemented to 0.5 mL with serum-free DMEM and were added to the plates. After 4 h, the medium was removed and the cells were washed three times with PBS. The cells were fixed in 4% formaldehyde/PBS for 10 min and then were washed again three times with PBS. Nuclei were stained with DAPI (2.0 μg/mL, Roche, Switzerland). After three washes with PBS, the cells were examined using a Carl Zeiss LSM 510 meta fluorescence microscope (Jena, Germany) with long focal length optics and excitation by He–Ne (543 nm) and argon ion (488 nm) lasers.

The uptake and release of peptide/DNA complexes from endosomes was examined in kinetic experiments performed using live cells. Briefly, NIH-3T3 cells were seeded in 15mm glass bottom culture dishes (NEST) containing glass cover slips (3×10^4 cells/mL)and were grown for 24 h. C_{18}-$C(LLKK)_3C$-TAT/DNA complexes were prepared as mentioned above. One microgram of plasmid was mixed with 2.5 μL YOYO-1 (10 μM). After 30 min at 37 °C, the peptide was added. The complexes were supplemented to 0.5 mL with the addition of serum-free DMEM, and after 4 h, the medium was removed and Lyso-Tracker Red (50 nM) was added. After 30 min, the cells were washed three times with PBS containing 2 mg/ml heparin sodium, and then were examined with a 60× oil immersion lens as described above in section **Calcein release assay in cells**.

Results and Discussion

Synthesis and Characterization of Peptides

Four conjugates containing a cationic amphiphilic α-helical AMP, $(LLKK)_3$, and the cell-penetrating peptide, TAT, were designed and synthesized to serve as gene vectors. The $(LLKK)_3$ segment was selected to mediate DNA binding of the peptides and endosomal escape, while TAT was included to promote gene packaging and delivery. To achieve a more compact condensation of DNA and efficient endosomal escape, some conjugates also contained a stearyl group or cysteine residues. To assess the role of these different moieties in peptide vectors, TAT, C18-TAT, $G(LLKK)_3G$, C18-$G(LLKK)_3G$, $C(LLKK)_3C$, and C18-$C(LLKK)_3C$ peptides were synthesized. The sequences for these peptides are listed in **Table 1.** These peptides were subsequently assayed for purity using analytical high performance liquid chromatography, and the purity of each was at least 95%.

Journal of Materials Chemistry B

Cite this: DOI: 10.1039/c0xx00000x

www.rsc.org/xxxxxx

Paper

Table 1 Sequence and molecular weight of the multifunctional peptides.

Peptide Name	Peptide Sequence	Molecular Weight	
		Calculated	Measured
TAT	GRKKRRQRRR-NH_2	1437.72	1439.10
G(LLKK)$_3$G	GLLKKLLKKLLKKG-NH_2	1621.17	1621.33
C(LLKK)$_3$C	CLLKKLLKKLLKKC-NH_2	1713.36	1717.22
G(LLKK)$_3$G-TAT	GLLKKLLKKLLKKGGRKKRRQRRR-NH_2	2999.83	3000.97
C(LLKK)$_3$C-TAT	CLLKKLLKKLLKKCGRKKRRQRRR-NH_2	3092.02	3093.28
C18-TAT	C_{18}-GRKKRRQRRR-NH_2	1662.17	1663.32
C18-G(LLKK)$_3$G	C_{18}-GLLKKLLKKLLKKG-NH_2	1844.90	1845.61
C18-C(LLKK)$_3$C	C_{18}-CLLKKLLKKLLKKC-NH_2	1937.80	1939.02
C_{18}-G(LLKK)$_3$G-TAT	C_{18}-GLLKKLLKKLLKKGGRKKRRQRRR-NH_2	3224.27	3225.84
C_{18}-C(LLKK)$_3$C-TAT	C_{18}-CLLKKLLKKLLKKCGRKKRRQRRR-NH_2	3316.46	3317.34

CD spectra

To investigate whether the introduction of the TAT peptide, stearyl group, and cysteine residues affected the ability of an α-helical structure to form in the peptides synthesized, peptide conformations were measured in aqueous solution, and in a 50% trifluoroethanol (TFE)/PBS (v/v) solution, using CD. The peptide CD spectra obtained in the latter solution were characterized by a minimum absorbance at 208 nm and a pronounced shoulder at 220 nm (Fig. 2A). These are typical signatures of a helical conformation. By establishing a cationic amphiphilic α-helical secondary structure in a hydrophobic environment, this structure has the potential to disrupt endosome membranes and promote the escape of peptide/DNA complexes from endosomes/lysosomes.[14-16] The conjugates without a stearyl group exhibited a high degree of random-coil conformations in PBS. In contrast, the stearylated conjugates tended to assemble into α-helical conformations, which is in accordance with the literature[19,20,26] and our hypothesis. By providing a hydrophobic environment, a stearyl group can promote AMPs to adopt an α-helical conformation. The α-helical content of the peptides containing cysteine residues was also generally higher than that of the peptides without cysteine residues, possibly due to the increased size of the former. The increase in size could enhance hydrogen bonding between the carbonyl O atom of an amino acid position (*i*) and the subsequent amide proton of the (*i*+ 4) amino acid position in the peptide backbone. This is highly probable since cysteine does not belong to the group of amino acids which have been shown to disrupt helices. Furthermore, an increased number of repeat units (n) could also increase α-helical folding by the same virtue.[22] The electrostatic repulsion of the lysine and arginine residues in the TAT segment was found to reduce the α-helical content slightly (Table S1). CD spectra showed that the incorporation of a stearyl group and cysteine residues promoted the formation of an amphiphilic α-helix conformation, with the hydrophobic leucine and hydrophilic lysine residues present on both sides of the conjugates. Since cationic amino acids tend to bind anionic DNA, and hydrophobic leucine residues bind the lipid cellular membrane[21], the presence of an amphiphilic α-helix conformation in the conjugates was consistent with the observation that the peptide/DNA complexes were able to compactly bind DNA and escape from endosomes and lysosomes.

Agarose Gel Electrophoresis Assays

To evaluate the DNA binding ability of the synthesized peptides, and thus their ability to provide efficient gene delivery, gel retardation assays were performed. The TAT and AMP sequences alone, as well as the C_{18}-TAT and C_{18}-AMP sequences containing cysteine residues, were evaluated. As shown in Fig. S1, TAT did not form a stable complex with DNA, even when the N/P ratio was as high as 3. In contrast, C_{18}-TAT retarded DNA migration at a N/P ratio of 2. The G(LLKK)$_3$G peptide retarded DNA migration at a N/P ratio of 3, while C(LLKK)$_3$C and G(LLKK)$_3$G-TAT (Fig. 3A) retarded DNA migration with N/P ratios of 2.5. Furthermore, C(LLKK)$_3$C-TAT exhibited a higher DNA binding capacity than C(LLKK)$_3$C and G(LLKK)$_3$G-TAT (Fig. 3B). Overall, these data indicate that increasing the length of a cationic peptide (e.g., by fusing TAT and (LLKK)$_3$), or linking peptides via disulfide bonds, results in an enhanced DNA binding ability. The other stearylated conjugates exhibited a high DNA binding capacity, with C_{18}-G(LLKK)$_3$G binding DNA when the N/P ratio reached 2.5. In comparison, C_{18}-G(LLKK)$_3$G-

TAT (Fig. 3C) and C_{18}-G(LLKK)$_3$G-TAT (Fig. 3D) bound DNA most efficiently at a N/P ratio of 2. Thus, the addition of a hydrophobic stearyl group was found to markedly improve DNA binding, with the stearylated peptides assembling via hydrophobic interactions and increasing the local charge density. The presence of the stearyl group also promoted the formation of an α-helical conformation. In this structure, the hydrophobic leucine residues assembled along the inside of the helical structure and the cationic lysine residues arranged along the outer hydrophilic side, thereby enhancing DNA-peptide interactions. Overall, the conjugates that were composed of the four functional segments were found to form stable complexes with DNA.

Particle Size and Zeta Potential

Particle size and zeta potential of peptide/DNA complexes has been shown to influence cellular uptake, the endocytosis pathway, nuclear entry, and transfection efficiency.[8] As shown in Fig. 4A, particle size of the peptide/DNA complexes decreased as the N/P ratio increased, up to a N/P ratio of 6. For example, the average particle size of the C(LLKK)$_3$C-TAT/DNA, C_{18}-G(LLKK)$_3$G-TAT/DNA, and C_{18}-C(LLKK)$_3$C-TAT/DNA complexes decreased from 200 nm in diameter to 90 nm in diameter as the N/P ratios increased from 2 to 6. The diameters then increased slightly to approximately 110 nm at a N/P ratio of 8. Meanwhile, the particle size of the G(LLKK)$_3$G-TAT/DNA complex was much larger than that of the others at identical N/P ratios. This can be ascribed to the N-terminal stearylation and the presence of cysteine residues which caused the peptide to aggregate due to the hydrophobic interactions that occurred among the stearyl groups and the more intense charge distribution as described above.

An appropriate particle size also needs to accompanied by the presence of positive charges on the surface of peptide/DNA complexes in order for these complexes to undergo endocytosis into the cytoplasm. As shown in Fig. 4B, the peptide/DNA complexes generated in this study exhibited an increasing trend in zeta potential as the N/P ratio increased. N-terminal stearylation further increased the zeta potential, and this increase was more significant than that for the addition of cysteine residues. Since the particle size and zeta potential of peptide/DNA complexes are crucial for gene delivery, the present results indicate that N-terminal stearylation and the addition of cysteine residues favor gene transfection.

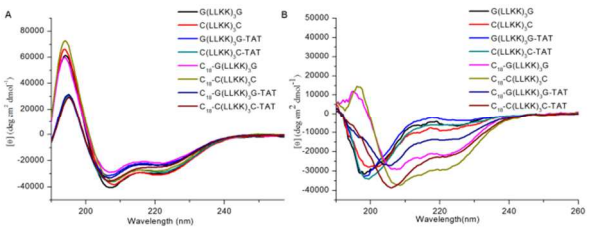

Fig.2 CD spectra of the peptides (each at a concentration of 50 μM) in 50% TFE/PBS solution (A) or PBS buffer alone (B).

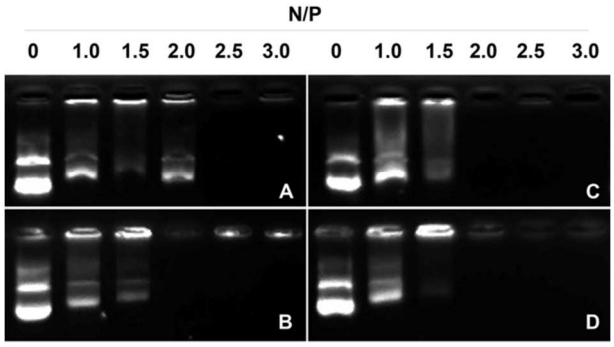

Fig.3 Agarose gel electrophoresis retardation assay for different N/P ratios of: (A) G(LLKK)$_3$G-TAT, (B) C(LLKK)$_3$C-TAT, (C) C_{18}-G(LLKK)$_3$G-TAT, and (D) C_{18}-C(LLKK)$_3$C-TAT.

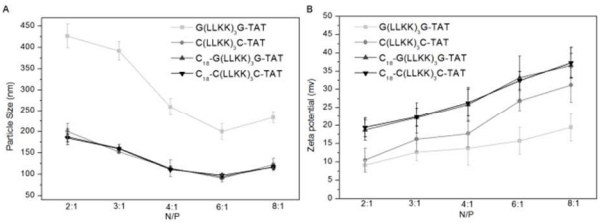

Fig.4 Particle size (A) and zeta potential (B) for the peptide/DNA complexes at different N/P ratios.

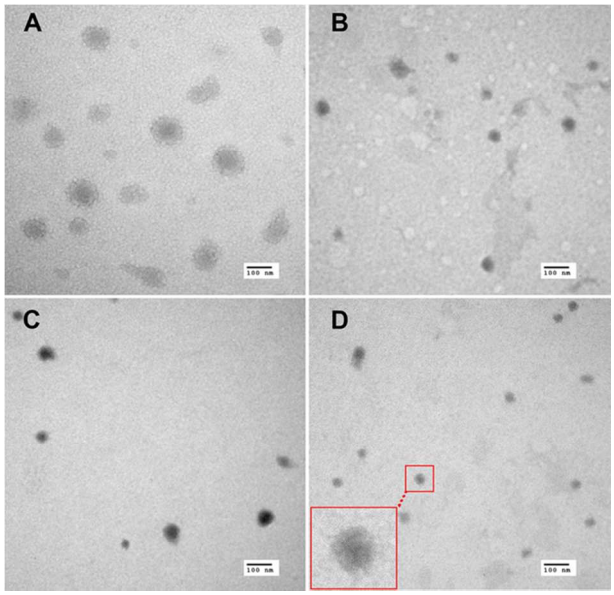

Fig. 5 TEM micrographs of the following peptide/DNA complexes at an N/P ratio of 4: (A) G(LLKK)$_3$G-TAT/DNA, (B) C(LLKK)$_3$C-TAT/DNA, (C) C_{18}-G(LLKK)$_3$G-TAT/DNA, and (D) C_{18}-C(LLKK)$_3$C-TAT/DNA. Scale bar: 100 nm.

Morphology of Peptide/DNA Complexes

The morphology of peptide/DNA complexes at an optimal N/P ratio (described in the next section) was observed with TEM. In Fig. 5, TEM micrographs of the peptide/DNA complexes at a N/P ratio of 4 are shown. Most of the peptide/DNA complexes displayed uniform spherical shape with an average size that ranged from ~37 nm to ~110 nm, which is smaller than that measured by DLS. The latter observation is due to the dried state of the TEM samples, whereas the DLS samples were in aqueous medium. As shown in Fig. 5, the particle size of the C(LLKK)$_3$C-TAT/DNA complex was smaller than that of the G(LLKK)$_3$G-

TAT/DNA complex, was similar with that of the C_{18}-G(LLKK)$_3$G-TAT/DNA, yet was larger than that of C_{18}-C(LLKK)$_3$C-TAT/DNA complexes, consistent with the DLS measurements. A size distribution analysis was provided in Fig. S2. These results indicate that N-terminal stearylation and the addition of cysteine residues facilitate compact DNA condensation by a peptide, followed by formation of stable, uniform sphere-shaped complexes.

Transfection efficiency

All of the conjugates were also evaluated for luciferase gene transfection of 293T and NIH-3T3 cells at different N/P ratios, and were compared with Lipo2000. Gene transfection efficiency was found to increase when functional moieties were added to the conjugates, and a 4:1 N/P ratio of conjugate to DNA was found to be optimal for luciferase gene expression by all of the conjugates. For the transfection of 293T cells with C_{18}-C(LLKK)$_3$C-TAT, the transfection efficiency (4.8×10^8 RLU/ mg protein) was 6.8-, 37-, and 1134-fold higher than that of C_{18}-G(LLKK)$_3$G-TAT, C(LLKK)$_3$C-TAT, and G(LLKK)$_3$G-TAT, respectively (Fig. 6 A). On the other hand, the transfection of 293T cells with C_{18}-G(LLKK)$_3$G-TAT at the same N/P ratio was 45-, 198-, 1289-, 3062-, 5000- and 3500-fold more efficient than C_{18}-C(LLKK)$_3$C, C_{18}-G(LLKK)$_3$G, C_{18}-TAT, C(LLKK)$_3$C, G(LLKK)$_3$G, and TAT peptides, respectively (Fig. 6C). A similar trend was observed with the transfection of NIH-3T3 cells (Fig. 6B and 6D). Moreover, at a N/P ratio of 4, C_{18}-C(LLKK)$_3$C-TAT-mediated transfection of 293T cells was 1.5-fold higher than that of Lipo2000. Of all the conjugates assayed, C_{18}-C(LLKK)$_3$C-TAT, which contained all of the functional moieties studied, was found to have the highest transfection efficiency. For example, transfection by C_{18}-G(LLKK)$_3$G–TAT was 29 times more efficient than C_{18}-TAT alone at a N/P ratio of 4 in 293T cells, with C_{18}-TAT observed to bind DNA and mediate cellular uptake of the complex (Fig. 3B). Similarly, the efficiency of transfection by C_{18}-G(LLKK)$_3$G–TAT in 293T cells was 136 times greater than that for G(LLKK)$_3$G–TAT, and this is potentially due to the difference in particle size (Fig. 4A and Fig. 5) and zeta potential (Fig. 4B) for the two peptides. The stearyl group also improved the association of the conjugate with the cellular membrane and promoted escape efficiency. In addition, the presence of cysteine residues affected the gene delivery performance of the conjugates. For example, transfection of 293T cells by C_{18}-C(LLKK)$_3$C-TATwas 6.8 times more efficient than C_{18}-G(LLKK)$_3$G-TAT, while C_{18}-C(LLKK)$_3$C transfected 293T cells with a 4.5-fold higher efficiency than C_{18}-G(LLKK)$_3$G. Taken together, these results support the hypothesis that biofunctional moieties play important roles in influencing transfection efficiency of peptide/DNA complexes.

Cellular uptake and translocation of peptide/DNA complexes

The gene transfection efficiency of non-viral vectors is related to cellular uptake, endosomal escape, and nuclear transfer.[30] To evaluate the gene delivery capacity of the moieties studied, cellular uptake of YOYO-1-labeled plasmid DNA complexed with each peptide at an optimal N/P ratio of 4 was assayed using FACS and confocal microscopy. Fig. 7 presents the DNA uptake data for the NIH-3T3 cells. The uptake level mediated by the stearylated conjugates (Fig. 7B) was generally higher than that mediated by the corresponding non-stearylated conjugates (Fig. 7A). Similarly, an increase in the length of a cationic peptide, e.g., by fusing TAT and (LLKK)$_3$ together, or by linking peptides via a disulfide bond to promote gene delivery, were associated with a higher uptake. For example, the mean fluorescence intensity of YOYO-1-labeled plasmid DNA delivered by C_{18}-C(LLKK)$_3$C-TAT (481.16 RLU) or C(LLKK)$_3$C-TAT (374.74 RLU) was much higher than that of Lipo2000 (237.29 RLU).

Using a confocal laser scanning microscope, uptake of labeled peptide/DNA complexes was also assayed (Fig. S3, S4). Both 293T cells and NIH-3T3 cells were incubated with different conjugates for 4 h, and the plasmid DNA and nuclei were labeled with YOYO-1 (green) and DAPI (blue), respectively. The images obtained showed that almost all of the peptide/DNA complexes, except G(LLKK)$_3$G-TAT/DNA, were internalized into nearly 100% of the treated cells, and some localized to the nucleus. Levels of green fluorescence increased in the following order: G(LLKK)$_3$G-TAT < C(LLKK)$_3$C-TAT < C_{18}-G(LLKK)$_3$G-TAT ≈ C_{18}-C(LLKK)$_3$C-TAT. Therefore, both FACS and confocal microscopy data verified the hypothesis that a stearyl moiety significantly enhances plasmid DNA delivery. Furthermore, the incorporation of cysteine residues, or the fusion of (LLKK)$_3$ and TAT segments, promotes the entry complexes into a cell. This is probably because the conjugates that contain these biofunctional segments efficiently condense the DNA into nanoparticles with a suitable particle size and zeta potential. The cellular uptake results are also consistent with the *in vitro* transfection data, and thus, they partly explain the high transfection efficiency that was observed for C_{18}-C(LLKK)$_3$C-TAT.

Cellular Uptake Pathway for the Complexes

Before evaluating endosomal escape efficiency, cellular uptake mechanisms were investigated using the following endocytosis-specific inhibitors: CPZ for clathrin-mediated endocytosis, MβCD for caveolin-mediated endocytosis, and amiloride for macropinocytosis. In FACS assays of NIH-3T3 cells, MβCD was found to decrease the cellular uptake of the peptide/DNA complexes most significantly (Fig. 8), while CPZ and amiloride also decreased cellular uptake. The effect of these endocytosis inhibitors on the transfection efficiency of the conjugates was also investigated in both 293T and NIH-3T3 cells. As shown in Fig. 9, treatment with MβCD was found to significantly decrease the transfection efficiency of the conjugates, while treatment with CPZ or amiloride also decreased luciferase activity, consistent with the FACS analysis data. The luciferase activity data showed that the transfection efficiency decreased sharply with the content of peptide in cells decreasing, because the endosomal escape is closely related with the peptide content. In combination, these results indicate that peptide/plasmid complexes are internalized into cells mainly via caveolin-mediated endocytosis, and partially via clathrin-mediated endocytosis and macropinocytosis. This may be due to the particle size of the complexes. For example, nanoparticles with a size of ~120 nm are internalized into cells primary by caveolin-mediated endocytosis, while a particle size of ~60 nm is internalized into cells primarily via clathrin-mediated endocytosis. A particle size larger than 500 nm is internalized primarily via macropinocytosis.[8] The average particle size of the peptide/DNA complexes in the present study ranged from 110 nm to 120 nm at a N/P ratio of 4, which would

be compatible with caveolin-mediated endocytosis. Alternatively, the cellular uptake that occurred via clathrin-mediated endocytosis or macropinocytosis was probably due to a smaller particle size and aggregation, respectively.

To investigate the endosomal escape of the functional fragments, transfection of $C(LLKK)_3C$-TAT/pGL3 and C_{18}-$C(LLKK)_3C$-TAT/pGL3 were performed in the presence and absence of CQ in 293T and NIH-3T3 cells.[31] As shown in Fig. S5 A and B, luciferase expression of $C(LLKK)_3C$-TAT/pGL3 at a N/P ratio of 4 in the presence of CQ was approximately 5-fold higher than in the absence of CQ. In contrast, luciferase expression of C_{18}-$C(LLKK)_3C$-TAT/pGL3 at a N/P ratio of 4 was only 1.2-fold higher in the presence versus the absence of CQ. In addition, an 8-fold increase in transfection efficiency was observed for C_{18}-TAT in the presence of CQ (data not shown). Overall, these experiments further demonstrate that the peptides of these conjugates mediate cellular uptake by endocytosis, and stearylated peptides undergo endosomal escape more efficiently. It is hypothesized that the latter observation is due to the association of the stearyl group with the hydrophobic membrane, which serves to increase the cellular uptake of the complexes in combination with the membrane disrupting ability of AMPs[16]. Thus, stearylated peptides have the potential to mediate gene transfection independent of CQ.

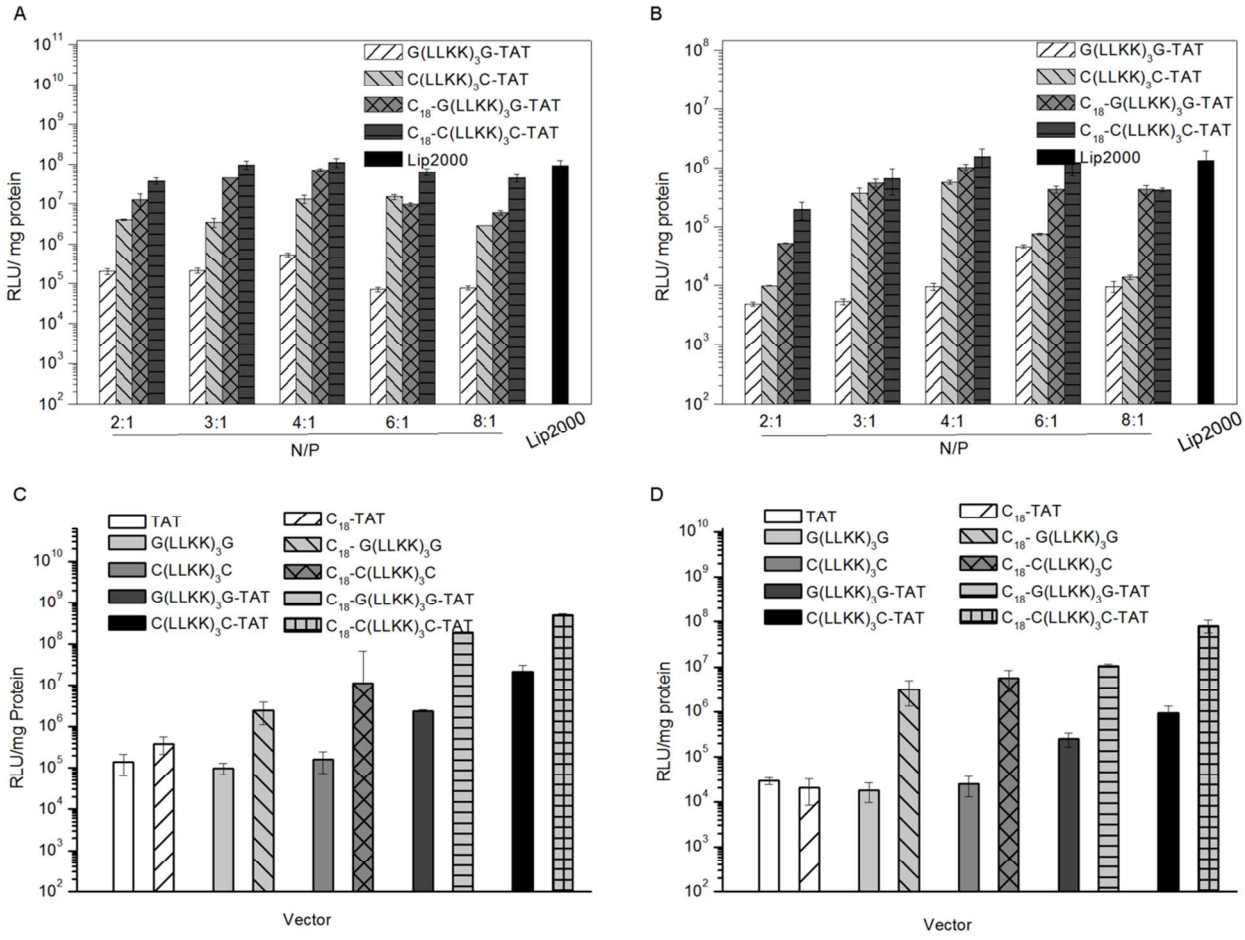

Fig. 6 *In vitro* luciferase expression levels in 293T cells (A) and NIH-3T3 cells (B) mediated by $G(LLKK)_3G$-TAT, $C(LLKK)_3C$-TAT, C_{18}-$G(LLKK)_3G$-TAT, and C_{18}-$C(LLKK)_3C$-TAT at N/P ratios ranging from 2 to 8. Luciferase expression levels for each of the biofunctional peptide segments at a N/P ratio of 4 in 293T cells (C) and NIH-3T3 cells (D). Data shown are the mean ± SD (n = 3).

Endosomal Lytic Activity

Endosomal lytic activity is crucial for gene transfection. In this study, calcein release assays were used to evaluate the endosomal lytic activity of the peptides tested. In control 293T and NIH-3T3 cells (e.g., those treated with calcein alone), punctuate fluorescence was only observed in the intracellular vesicles (Fig. 10, A1 and B1), thereby indicating that calcein was internalized into endosomes. When the peptides were incubated with each of the cell lines in parallel, greater fluorescence was observed in the cytoplasm (A2-A5 and B2-B5, respectively), indicating that the peptides were able to undergo endosomal escape.

To quantitatively evaluate the membrane disrupting capability of the peptides of interest, liposome leakage assays were conducted. Using peptides and peptide/DNA complexes (N/P = 4) with calcein liposomes, C_{18}-$G(LLKK)_3G$-TAT and C_{18}-$C(LLKK)_3C$-TAT were found to possess high membrane lytic activity (Fig. S6), compared with the complete lysis of liposomes that was achieved in the presence of Triton X-100 (the positive control). However, the percentage of lytic activity of the $C(LLKK)_3C$-TAT and $G(LLKK)_3G$-TAT peptides without a stearyl group were 40.22% and 25.35%, respectively. The membrane activity of the peptide/DNA complexes were slightly lower than the corresponding peptides alone, although the percentage of lytic

activity for the C_{18}-G(LLKK)$_3$G-TAT/DNA and C_{18}-C(LLKK)$_3$C-TAT/DNA complexes were 58.83% and 72.21%, respectively. Both C_{18}-C(LLKK)$_3$C-TAT and the C_{18}-C(LLKK)$_3$C-TAT/DNA complex exhibited the highest membrane lytic activity, thereby indicating a high endosomal escape efficiency.

Kinetics of the uptake and release of peptide/DNA complexes from endosomes was examined in living cells. NIH-3T3 cells that were treated with C_{18}-C(LLKK)$_3$C-TAT/pGL3 DNA complexes for 1 h or 4 h were observed by confocal laser scanning microscopy. As shown in Fig. 11**,** a small percentage of the C_{18}-C(LLKK)$_3$C-TAT/DNA complexes were internalized into cells after 1 h, and these complexes localized to lysosomes (indicated with the yellow fluorescence). In contrast, a large percentage of the C_{18}-C(LLKK)$_3$C-TAT/DNA complexes were internalized after 4 h, and these complexes remained evenly distributed in the cytoplasm. Only a few complexes remained entrapped in lysosomes. Taken together, these results indicate that C_{18}-C(LLKK)$_3$C-TAT is able to efficiently translocate plasmid DNA into cells via endocytosis, and these complexes are able to undergo endosomal escape.

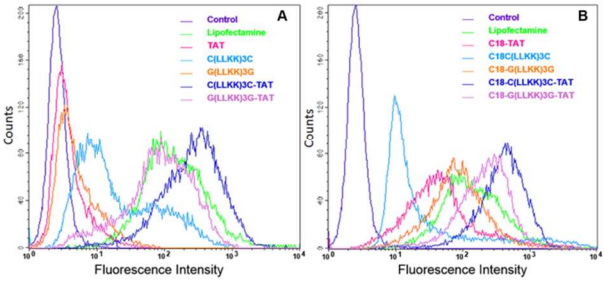

Fig.7 Cellular uptake of non-stearylated peptide/DNA complexes (A) and stearylated peptide/DNA complexes (B) in NIH-3T3 cells using flow cytometry. The plasmid DNA was labeled with YOYO-1 and was complexed with each peptide at the optimal N/P ratio of 4.

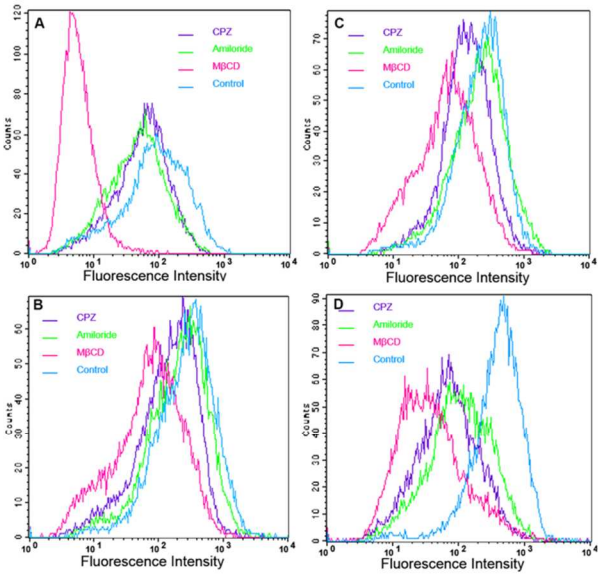

Fig.8 FACS assay of cellular uptake pathways mediated by G(LLKK)$_3$G-TAT/DNA (A), C(LLKK)$_3$C-TAT/DNA (B), C_{18}-G(LLKK)$_3$G-TAT/DNA (C), and C_{18}-C(LLKK)$_3$C-TAT/DNA (D) complexes, each at a N/P ratio of 4 in NIH-3T3 cells in the presence of endocytosis-specific inhibitors.

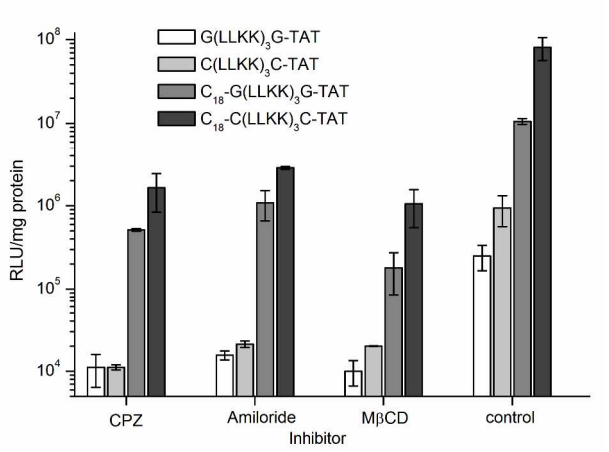

Fig.9 Transfecion activity of the peptide/DNA complexes studied as detected in the presence of endocytosis inhibitors. Peptide/pGL3 complexes were at a N/P ratio of 4 in 293T cells (A) and NIH-3T3 cells (B) in the presence of endocytosis-specific inhibitors as indicated.

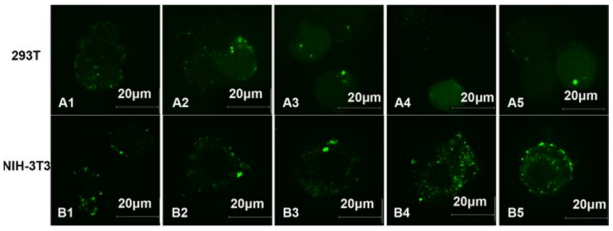

Fig.10 Calcein release assays performed in 293T and NIH-3T3 cells. Confocal microscopy images were obtained with calcein alone (A1, B1), with calcein/G(LLKK)$_3$G-TAT (A2, B2), with calcein/C(LLKK)$_3$C-TAT (A3, B3), with calcein/C_{18}-G(LLKK)$_3$G-TAT (A4, B4), and with calcein/C_{18}-C(LLKK)$_3$C-TAT (A5, B5), respectively in each case. Scale bar: 20 μm.

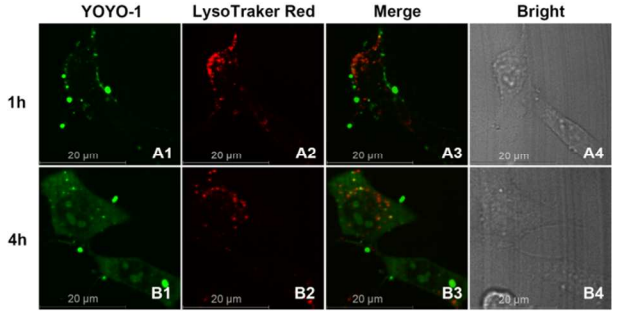

Fig.11 Cellular uptake and endosomal escape of C_{18}-C(LLKK)$_3$C-TAT/DNA complexes at a N/P ratio of 4. Confocal micoscopy images were obtained for C_{18}-C(LLKK)$_3$C-TAT/DNA complexes after 1 h (A1-A4) and 4 h (B1-B4) of treatment. The pGL3 plasmid was labeled with YOYO-1 (green signal, A1 and B1) and lysosomes were stained with LysoTracker Red (red signal, A2 and B2). An overlay of the A1 and A2 images are shown in A3, and an overlay of the B1 and B2 images are shown in B3. Scale bar: 20 μm.

Cytotoxicity

The biocompatibility of a gene delivery system is critical for successful gene transfection. To assess the potential cytotoxicity of the peptide/DNA complexes studied, an MTS assay was conducted using 293T and NIH-3T3 cells. As shown in Figure 12A and12B, no significant cytotoxicity was observed in either cell line for the four peptide/DNA complexes at N/P ratios ranging from 2 to 8. However, cell viability slightly decreased at a N/P ratio of 8 due to the high charge density. Cytotoxicity of the peptide materials was also evaluated and no significant

cytotoxicity was observed. Moreover, cell viability generally remained above 90% following the transfection of the peptide vectors (Figure 12C and 12D). Therefore, all of the complexes and conjugates exhibited much lower cytotoxicity compared with Lip2000/DNA complexes, with cell viability being greater than 90%.

Conclusions

In this study, a series of peptides containing diverse functional moieties were designed and synthesized in order to overcome various barriers to non-viral gene delivery. The peptides consisted of segments associated with cell penetration, endosomal escape, and DNA binding characteristics. It was confirmed that the presence of a stearyl groupand cysteine residues induced AMPs to assemble into amphiphilic α-helical conformations in PBS, and this was beneficial for the binding of DNA and cellular uptake. The peptide, C_{18}-C(LLKK)$_3$C-TAT, combined all of the functional moieties that were tested, and it exhibited the highest transfection efficiency. This transfection efficiency was also comparable to that achieved with Lip2000, yet was accompanied by lower levels of cytotoxicity and did not require a lysosomotropic agent due its high endosomal lytic capacity. To our knowledge, it is the first study to incorporate both a hydrophobic group and cysteine residues to induce an α-helical conformation in AMPs and to mediate gene delivery. Overall, the results obtained demonstrate that peptide bioconjugates have the potential to provide efficient gene delivery, and they provide a reference for the future design of peptide-based gene vectors.

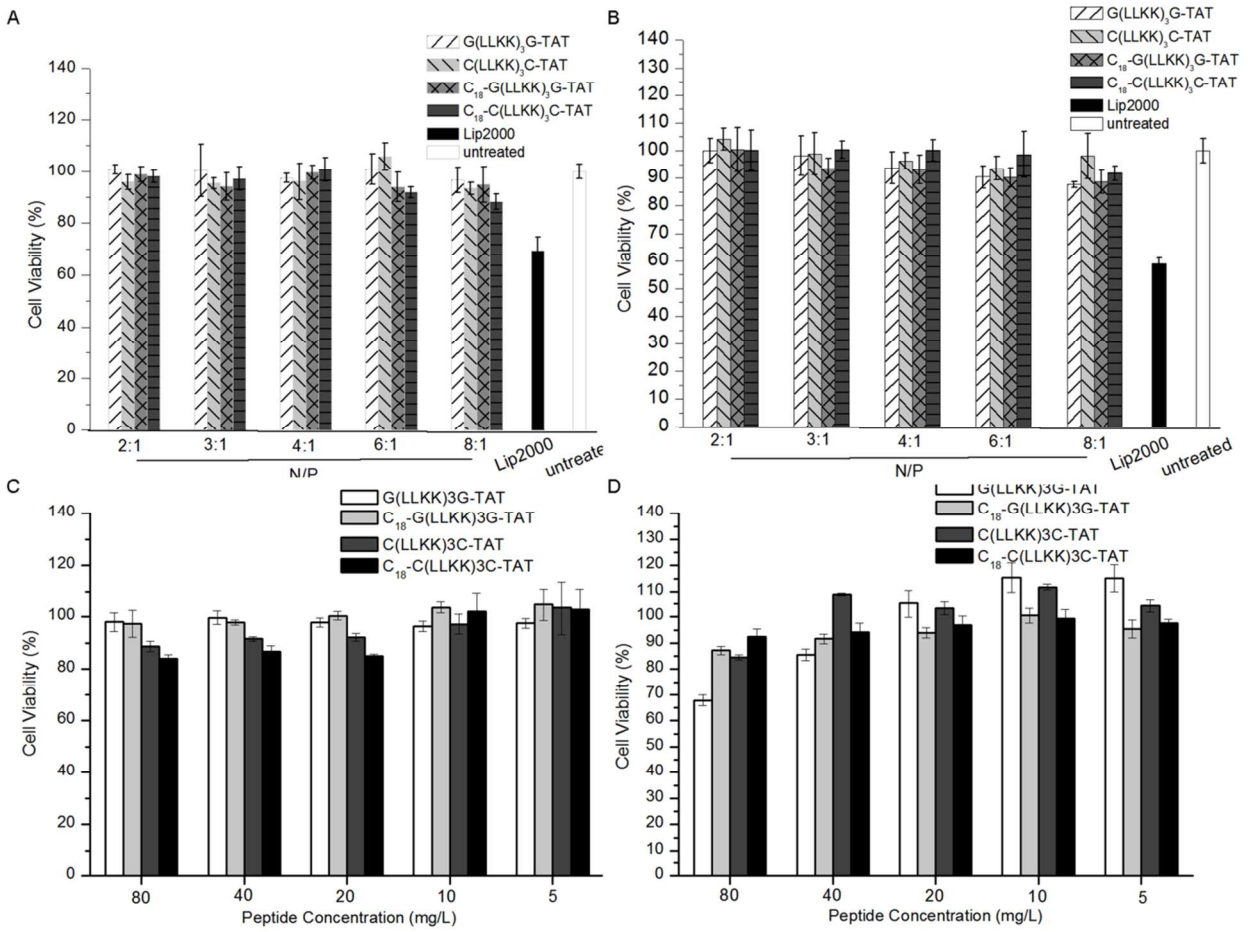

Fig.12 Cell viability of 293T cells (A) and NIH-3T3 cells (B) following treatment with peptide/DNA complexes at N/P ratios ranging from 2 to 8. Cell viability of 293T cells (C) and NIH-3T3 cells (D) following treatment with peptide concentrations ranging from 5 mg to 80 mg per liter. Lipofectamine 2000 (Lip 2000) was used as a positive control. Data shown are the mean ± SD (n = 5).

Acknowledgements

This work was supported by the National Natural Science Foundation of China (81202465 and 51373080) and the National Key Technologies R & D Program for New Drugs of China (2012ZX09301003).

[a] *Beijing Institute of Pharmacology & Toxicology, Beijing, 100850, PR China. Fax: +86-10-68211656; Tel.: +86-10-68169363; E-mail: keliangliu55@126.com (K. Liu)*

[b] *Key Laboratory of Functional Polymer Materials (Ministry of Education) and Institute of Polymer Chemistry, Nankai University, and Collaborative Innovation Center of Chemical Science and Engineering (Tianjin), Tianjin 300071, PR China. Fax: +86-22-23503510; Tel.: +86-22-23503509; E-mail: yanhs@nankai.edu.cn (H. Yan)*

† Electronic Supplementary Information (ESI) available: [details of any supplementary information available should be included here]. See DOI: 10.1039/b000000x/

References

1 S. L. Ginn, I. E. Alexander, M. L. Edelstein, M. R. Abedi, J. Wixon, J. *J gene med*, 2013, **15**, 65-77.
2 K. Han, S. Chen, W. H. Chen, Q. Lei, Y. Liu, R. X. Zhuo, X. Z. Zhang, *Biomaterials*, 2013, **34**, 4680-4689.
3 C. H. Jones, C. K. Chen, A. Ravikrishnan, S. Rane, B. A. Pfeifer, *Mol pharmaceutics*, 2013, **10**, 4082-4098.
4 R. Juliano, J. Bauman, H. Kang, X. Ming, *Mol pharmaceutics*, 2009, **6**, 686-695.
5 H. Soifer, C. Higo, C. R. Logg, L. J. Jih, T. Shichinohe, E. Harboe-Schmidt, K. Mitani, N. Kasahara, *Mol ther*, 2002, **5**, 599-608.
6 M. A. Mintzer, E. E. Simanek, *Chem Rew*, 2009, **109**, 259-302.
7 K. Gao, L. Huang, *Mol pharmaceutics,* 2008, 6, 651-658.
8 K. L. Dana Maria Copolovici, Elo Eriste, and Ulo Langel, *Acs Nano*, 2014, **8**, 1972-1994.
9 Y. S. Cho, G. Y. Lee, H. K. Sajja, W. Qian, Z. Cao, W. He, P. Karna, X. Chen, H. Mao, Y. A. Wang, L. Yang, *Small*, 2013, **9**, 1964-1973.
10 N. Ferrer-Miralles, E. Vazquez, A. Villaverde, *Trends Biotechnol,* 2008, **26**, 267-275.
11 F. Salomone, F. Cardarelli, M. Di Luca, C. Boccardi, R. Nifosì, G. Bardi, L. Di Bari, M. Serresi, F. Beltram, *J Controlled Release*, 2012, **163**, 293-303.
12 V. P. Torchilin, *Adv Drug Deliv Rev*, 2008, **6**0,548-558.
13 W. Y. Seow, Y.Y. Yang, *Adv Mater*, 2009, **21**, 86-90.
14 E. Wagner, *Adv Drug Deliv Rev*, 1999, **38**, 279-289.
15 C. Plank, W. Zauner, E. Wagner, *Adv Drug Deliv Rev*, 1998, **34**, 21-35.
16 A. K. Varkouhi, M. Scholte, G. Storm, H. J. Haisma, *J Controlled Release*, 2011, **151**, 220-228.
17 N. Toriyabe, Y. Hayashi, H. Harashima, *Biomaterials*, 2013, 34, 1337.
18 L. Tonges, P. Lingor, R. Egle, G. P. Dietz, A. Fahr, M. Bahr, *RNA*, 2006, **12**, 1431-1438.
19 K. N. B. Alexander F. Chu-Kung, Nathan A. Lockwood, Judith R. Haseman, Kevin H. Mayo, and Matthew V. Tirrell, *Bioconjugate Chem*, 2004, **15**, 530-535.
20 M. T. Ying-Ching Yu, Gregg B. Fields, *J Am Chem Soc.*, 1998, 120, 9979-9987.
21 Rajpal, A. Mann, R. Khanduri, R. J. Naik, M. Ganguli, *J Controlled Release*, 2012, **157**, 260-271.
22 N. Wiradharma, M. Khan, L. K. Yong, C. A. Hauser, S. V. Seow, S. Zhang, Y. Y. Yang, *Biomaterials*, 2011, **32**, 9100-9108.
23 J. Yang, H.-Y. Wang, W.-J. Yi, Y.-H. Gong, X. Zhou, R.-X. Zhuo, X.-Z. Zhang, *Adv Healthcare Mater*, 2013, **2**, 481-489.
24 S. L. Lo, S. Wang, *Biomaterials*, 2008, **29**, 2408-2414.
25 N. Wiradharma, U. Khoe, C. A. Hauser, S. V. Seow, S. Zhang, Y. Y. Yang, *Biomaterials*, 2011, **32**, 2204-2212.
26 Q. Meng, Y. Kou, X. Ma, L. Guo, K. Liu, *J Pept Sci*, 2014, **20**, 223-228.
27 K. Rittner, A. Benavente, A. Bompard-Sorlet, F. Heitz, G. Divita, R. Brasseur, E. Jacobs, *Mol Ther*, 2002, **5**, 104-114.
28 J. C. M. Stewart, *Anal Biochem*, 1980, **104**, 10-14.
29 W. Zhang, J. Song, R. Liang, X. Zheng, J. Chen, G. Li, B. Zhang, K. Wang, X. Yan, R. Wang, *Peptides*, 2013, **46**, 33-39.
30 L. Yin, Z. Song, K. H. Kim, N. Zheng, H. Tang, H. Lu, N. Gabrielson, J. Cheng, *Biomaterials*, 2013, **34**, 2340-2349.
31 S. Yang, D. J. Coles, A. Esposito, D. J. Mitchell, I. Toth, R. F. Minchin, *J Controlled Release*, 2009, **135**, 159-165.

Table of Contents Graphic

Peptide Amphiphiles with Multifunctional Fragments Promoting Cellular Uptake and Endosomal Escape as Efficient Gene Vectors

Liang Luan[a], Qingbin Meng[a], Liang Xu[a], Zhao Meng[a], Husheng Yan*[b] and Keliang Liu*[a]

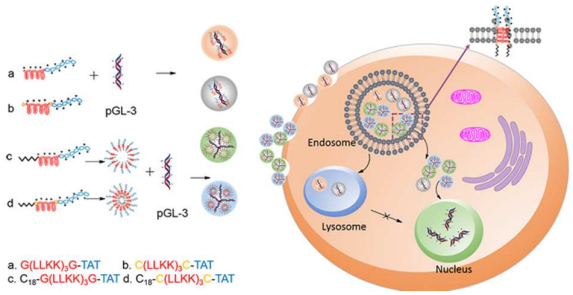

A series of peptides containing multiple functional fragments were designed as gene-delivery vectors with transfection efficiency comparable to Lipofectamine 2000.